

Handheld threat object identification performance of 2-D visible imagery versus 3-D visible imagery

Keith Krapels

Office of Naval Research
800 North Quincy Street
Arlington, Virginia 22217

Ronald G. Driggers

Brian Teaney

U.S. Army Night Vision and Electronic
Sensors Directorate
10221 Burbeck Road
Fort Belvoir, Virginia 22060

Carl Halford

University of Memphis
Center for Advanced Sensors
Memphis, Tennessee 38152

Abstract. This research determines if there is an improvement in human observer performance, identifying potential weapons or threat objects, when imagery is presented in three dimensions instead of two dimensions. The potential improvement in performance is quantified by evaluating the change in the N_{50} cycle criteria, for this task and target set. The data suggests that as much as a 30% improvement in range capability may result from using 3-D imagery. The advent of affordable, practical, and real-time 3-D displays has led to a desire to evaluate and quantify the performance trade space for this application of the technology. Imagery was collected using a dual-camera stereo imaging system. A series of eight different resolutions were presented to observers in both 2-D and 3-D formats. The set of targets consisted of 12 handheld objects. The objects were a mix of potential threats or weapons and possible confusers. For example, a cellular telephone and a hand grenade are two such objects. This target set is the same target set used in previously reported research that determined the N_{50} requirements for handheld objects for both visible and infrared imagers. © 2006 Society of Photo-Optical Instrumentation Engineers. [DOI: 10.1117/1.2209650]

Subject terms: target acquisition; modeling; performance; imaging.

Paper 050617R received Jul. 30, 2005; revised manuscript received Nov. 3, 2005; accepted for publication Nov. 21, 2005; published online Jun. 16, 2006. This paper is a revision of a paper presented at the SPIE Conference on Infrared Imaging Systems, March 2005, Orlando, Florida. The paper presented there appears (unrefereed) in SPIE Proceedings Vol. 5784.

1 Introduction

The motivation for studying this area is a desire to evaluate the use of three dimensional (3-D) imagery in antiterrorism/force protection (AT/FP) or asymmetric threat imaging scenarios. It has long been recognized by the intelligence community that there is a significant performance improvement for imagery analysts when using stereo pair 3-D imagery for intelligence tasks.

There is a confluence of factors that have led to this study. First is the development of a number of 3-D imaging architectures practical for tactical applications.¹ Second is the development of practical, inexpensive 3-D display technology.² Third is the need to re-evaluate sensor technology development, which began prior to the USS Cole bombing and September 11, 2001, in light of the increased emphasis on AT/FP, military operations in urban terrain (MOUT), and asymmetric threats (Chief of Naval Operations Guidance for 2005, Chief of Staff of the U.S. Army's Army Strategic Planning Guidance). The resulting successes on the unconventional and conventional battlefields of Iraq and Afghanistan indicate there is currently an overmatch in capability for these applications. However, the postinvasion period in Iraq, and the emphasis on increasing security capability at home [Department of Homeland Security (DHS) creation] and abroad indicate that it is appro-

priate to alter the performance goals for sensor technology development and re-evaluate technologies for application to asymmetric threat environments.

The 3-D imaging ladar developed by Army Research Laboratory's (ARL) Electro-optics and Photonics division is an example of these technologies. The Office of Naval Research has shared the development cost of this sensor technology with ARL, in an effort to create a multiuse sensor technology, that is, to create a technology that will perform classic symmetric threat tasking, such as laser ranging and tracking, and yet be capable of performing new tasks appropriate to the AT/FP mission, such as long-range, super-high-resolution, eyesafe, active imaging. In the asymmetric threat environment, there is not the classic penalty for actively illuminating objects/targets—giving away camouflaged/concealed positions. While originally this sensor architecture was developed for imaging under or through foliage and camouflage netting (a classic symmetric threat task), it appears to have great potential to be applied to the AT/FP and asymmetric threat imaging environment.

This research follows efforts at the U.S. Army Night Vision Lab to determine the task difficulty metrics for discriminating threatening handheld objects from nonthreatening ones. In 2003 and 2004 a series of experiments³⁻⁵ were conducted to evaluate the difficulty of discriminating these targets/objects by performing human observer object identification perception experiments. The perception experi-

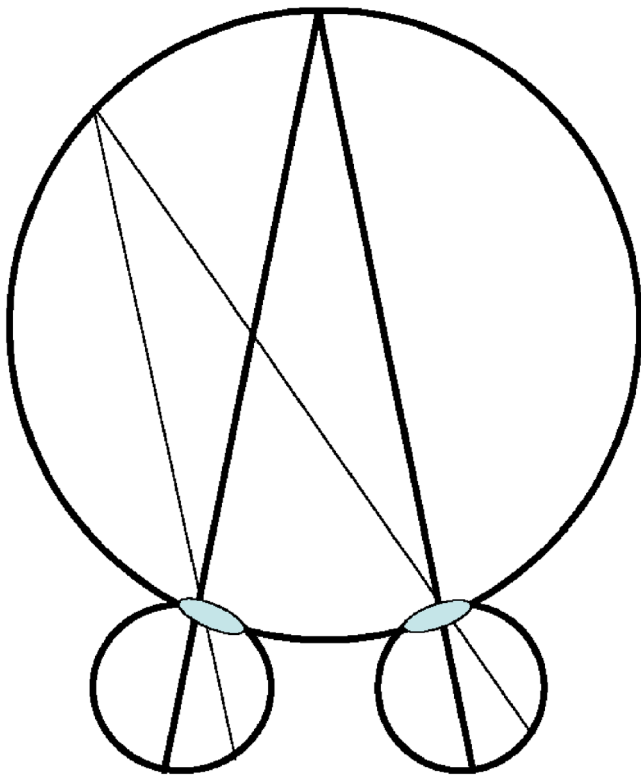


Fig. 1 Illustration of horopter.

ments were conducted with imagery from monochrome visible, midwave infrared and long-wave infrared sensors. All of these sensors imaged in two dimensions. The significant difference between this study and the previous ones was that the imagery was collected in both 2-D and binocular 3-D modes.

The U.S. Army Night Vision and Electronic Sensors Directorate (NVESD) experiments used two sets of targets/objects. The first set was objects held in two hands, e.g., rake or rifle, and the second set was objects held in a single hand, e.g., cell phone or pistol. The result from the analysis of the observer performance data is a task difficulty metric called the cycle criteria, N_{50} . This value describes the number of resolved cycles across the object's critical dimension D_{crit} required for an observer to have a 50% probability of successful task completion. The value N_{50} is different for the task and for the object set. Typical tasks modeled in the military target acquisition community are detection, recognition, classification, and identification. For example, it typically requires approximately twice as many resolved cycles on an object to identify it (T-62 tank versus M-1 tank) as it does to recognize it (tracked versus wheeled vehicle). For a more detailed description of this modeling process, and terms such as D_{crit} and N_{50} , see Ref. 6. In this case the task is identifying the object, from an ensemble of similar sized objects, which includes threatening and non-threatening ones.

This experiment used the same handheld objects used in the previous NVESD experiment. The previous experiment was focused on handheld object discrimination for police and force protection sensor design. This choice of object set was to facilitate comparison of the results to the previous

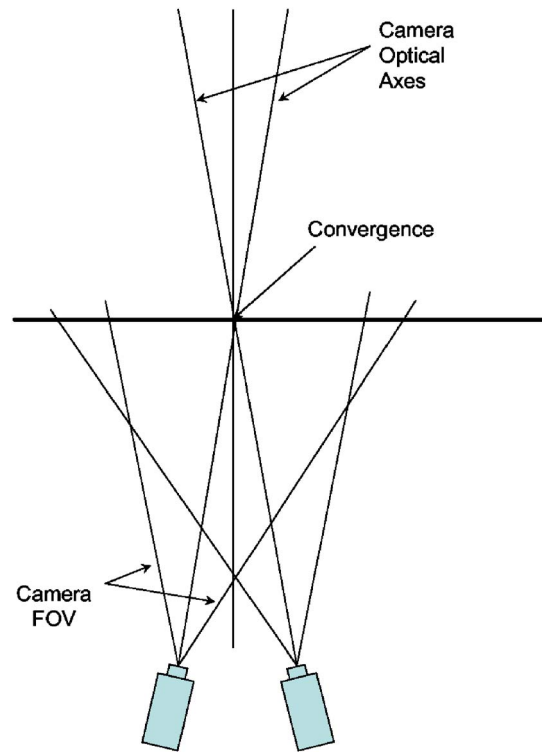


Fig. 2 Toed-in camera configuration.

work. The goal was to determine the value of 3-D imagery to improve identification performance of observers tasked to discriminate these objects. The analyses included comparing raw performance and derived N_{50} for the target ensemble/task.

The following sections of this paper begin with a review of the history of target acquisition modeling and a discussion of the theory, followed by a description of the experiment. The technique for calculating limiting frequency is then described. Raw results are provided and the derivation of the N_{50} value is then given. Finally, a section describes how N_{50} is used in the target acquisition model to provide probability of threat object identification.

2 Background: Target Acquisition Modeling

Currently, there is not an electro-optical system performance model for the design and/or analysis of system performance in the application of 3-D imagers used for target identification. There are two well-established military imaging performance models: target acquisition⁷ and surveillance/reconnaissance.⁸ The surveillance and reconnaissance model approach for 3-D object identification would require the development of a National Imagery Interpretability Rating Scale (NIIRS) scale for asymmetric threat objects and the development of a general image quality equation (GIQE) for these threats. In addition, the GIQE has four parameters that must be calibrated for the equation. In contrast, the target identification model has been shown to be successfully applied to various target sets. Also, the only calibration requirement for application to 3-D object imagery is the determination of a 50% probability of identification cycle criterion. This criterion, along



Fig. 3 Handheld objects.

with a minimum resolvable contrast (MRC) model for the electro-optical system, enables the probability of object identification to be calculated for any 3-D electro-optical system. Therefore, the imaging systems mentioned above could be evaluated for threat object identification using 3-D imagery. In this research, we have initiated the experiments to evaluate this 3-D imaging technology and its application to this particular military task and derive cycle criterion for threat object identification.

Johnson, of the NVESD, proposed the seminal hypothesis for the U.S. Army's target acquisition model in 1958.⁹ Johnson proposed that the ability of an observer to acquire military targets in scenes was dependent on how well he could resolve bar patterns of varying frequencies through the device at the same contrast as the scene target-to-background contrast.

Johnson performed the following experiment.¹⁰ Scale models of eight different vehicles and one soldier were placed against a bland background in the laboratory. Observers viewed the targets through image intensifiers, and they performed detection, recognition, and identification tasks. Air Force three-bar charts with the same contrast as the scale targets were used to establish the limiting light performance of the image intensifiers. By this means, the maximum number of resolvable cycles across the target minimum dimension was determined for each task.

It was found that the number of just-resolvable cycles across the minimum dimension of each target required to perform each task was within 25% of a fixed number of cycles. For the particular set of targets used, 1.0 cycle was

needed for detection, 4.0 cycles for recognition, and 6.4 cycles for identification. These cycle criteria (N_{50}) are for a 50% success rate. In this manner, the ability of the observers to perform target discrimination tasks was related to their ability to resolve bar patterns.

Lawson, Ratches, Johnson, and others evolved a target-acquisition, range-performance model based on Johnson's work.¹¹⁻¹⁵ In the more recent target acquisition models, the square root of the target presented area was used rather than the minimum dimension.^{16,17} This change had two virtues. First, the original model used only the horizontal resolution of the sensor to predict performance, whereas the newer model used both the horizontal and vertical characteristics of the sensor. Second, the improved range performance that occurred when viewing a tactical vehicle from the side was then predicted by the model. The original model was also changed to incorporate the limitations of the human eye.^{18,19}

The cycle criteria generally used today are based on experiments with visible and thermal images of ground targets, aircraft, etc. The N_{50} values depend on the target set;

Table 1 Processed image file naming convention/experimental matrix.

Image type	Gaussian blur (pixels)							
	15	24	33	42	51	60	69	78
2-D	AA	AB	AC	AD	AE	AF	AG	AH
3-D	BA	BB	BC	BD	BE	BF	BG	BH

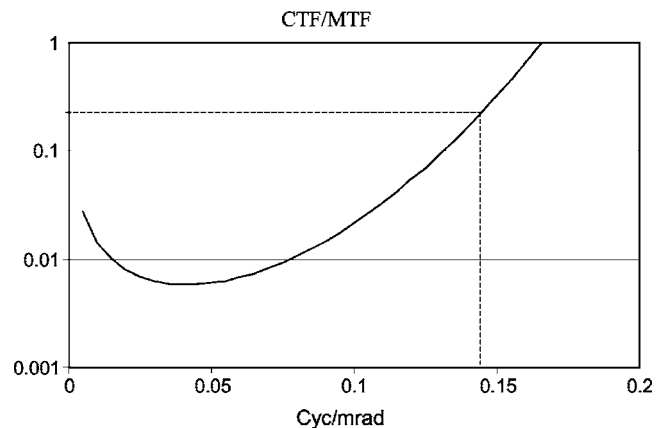


Fig. 4 The effective CTF is the human CTF divided by the system MTF. The limiting frequency that can be seen for a given contrast level occurs at the intersection of the CTF/MTF curve and the contrast level.

Table 2 Target characteristics.

	Contrast average	Contrast std. dev.	Characteristic dimension average	Characteristic dimension std. dev.	Object size observer space (mrad)
Side view	0.253	0.094	121.0	31.3	37.2
Front view	0.205	0.074	107.2	31.4	33.0
All views	0.229	0.086	114.1	31.4	35.1

that is, N_{50} for recognition and identification increases if the targets look alike and N_{50} decreases if the targets have dissimilar shapes. Also, experience over the years seemed to indicate that the cycle criteria varied with sensor type (thermal versus image intensifier versus visible). However, the experiment described here is the first quantitative comparison of N_{50} in the application of 3-D threat object identification.

The objective of this research is to derive N_{50} values for 3-D threat objects in the visible band. A threat object target set (for testing in an identification task) was used with visible images, the images were blurred, and a perception experiment was performed to determine the N_{50} values associated with the target set. Note that the experiment was performed for an ensemble of observers against an ensemble of targets.

3 Theory: 3-D Vision

The binocular or 3-D visual system comprises a zone in which both of the eyes pick up slightly different views of the same scene and the brain is able to combine them to create one coherent image. This zone is termed the horopter and is comprised of the center of the “field of view” of the eyes. Figure 1 depicts the theoretical horopter, in which the stereo effect is visible.

Within this zone, the disparate images allow us to perceive various cues such as depth, spatial locality, and distance. The name given to this appearance of the cues generated by this binocular disparity is stereopsis.

Capabilities to visualize stereo processes are not uniform throughout the population. Every human has a subtle variation in interocular separation, which is the main factor affecting the capture and processing of stereo images. For this particular experiment we used a camera separation of 2.5 in., to simulate the average intereye separation for the human.²⁰ The potential for painful divergent stereo images does exist in this case for persons with a smaller separation, but a reasonable difference was selected for the study. A toed-in camera configuration was used (shown in Fig. 2), which resulted in some minor keystone affect; however, the presence of incongruities in the sides of the images were irrelevant as the objects themselves were present in the center of the scene, thus mitigating any negative effects of this particular camera configuration.

Stereoscopic research is fundamentally concerned with the processes of detection and recognition. Previous studies have proven the benefits of stereo camera configurations for these tasks.²¹ However, little work has been performed in terms of benefits of stereo in terms of object identification.

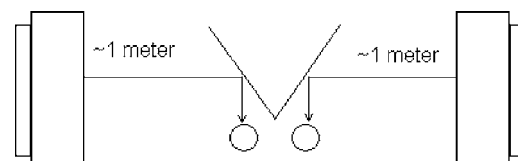
In proceeding with this object identification study, the aim is to establish a starting point for evaluating and modeling the perceptual processes associated with stereo identification tasks. The main perceived benefit for stereo vision in object identification is the presence of volumetric cues in the images. These cues give indications as to the shape, features, and aspect of the object in question. These volumetric cues are what ultimately cause the images to “pop” out at the observer and are notably helpful in object detection tasks. A second, more obvious, benefit is the addition of a second image to the observer. Given the shift-variant nature of imagers, the presence of a second image gives a different picture of the scene altogether. This second scene may in turn provide additional useful information to the observer that can be used to positively identify the target.

4 Imagery Collection and Preparation

Twelve handheld objects were used in this experiment, where the objects are shown in Fig. 3. From top left to bottom right, the objects were a brick, camera, cell phone, flashlight, grenade, pistol, knife, coffee cup, personal digital assistant, rock, soda can, and a radio.

Both 2-D and 3-D imagery was obtained of these 12 targets for two aspects. The first aspect was normal to the hand as shown in Fig. 3. The second aspect was parallel to the hand (at a right angle to the objects shown). All of the images were taken in the visible band and were obtained with a Canon E60 high-resolution camera. The image size was 2048 by 1360 and the images were taken outside with natural illumination. The images were obtained in color, but were converted to gray scale for the experiment and down-sampled to 768 by 512 image elements.

The images were prepared, sorted, and named for the experiment using the experimental matrix shown in Table 1. Each of the 12 targets, imaged from two aspects, was blurred to various levels of blur ranging from 15 to 78 pixels. For example, the 24 images in cell “BF” were 3-D and had been convolved with a Gaussian blur 60 pixels in width. Each cell in the experimental grid contained 24 images with a common level of blur. The overall

**Fig. 5** Perception experiment hardware layout.

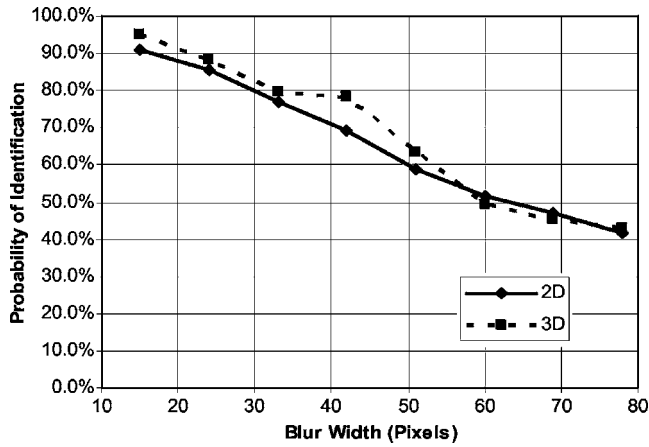


Fig. 6 Probability of object identification versus blur—all 10 observers.

experimental matrix included 384 images (12 targets×2 aspects×8 blurs for both 2-D and 3-D). The blur was imposed on the images with a Gaussian function that was convolved with the images. This simulates increased range or concurrently decreased resolution on target. Equation (1) is the functional form of the Gaussian,

$$f(x,y) = \exp\left[-\pi\left(\frac{\sqrt{x^2+y^2}}{b}\right)^2\right] \quad (1)$$

where b is in pixels. The number of pixels associated with each blur, in the experimental cells of Table 1, is given across the top of the matrix. The images were not presented to the observers in groups of the cells shown. The entire array of 384 images was randomized so that the observers did not tire of a particular blur level.

5 Performance Modeling

The experiment performed in this research included no temporal noise and the limiting frequency of each process was determined by the contrast threshold function (CTF) of the eye and experimental blur imposed on the imagery. The CTF changed with average display luminance and spatial frequency. For the CTF equation, which is an empirical fit to an ensemble of observers, see Ref. 18. The reduction in contrast by the experimental blur included both the modu-

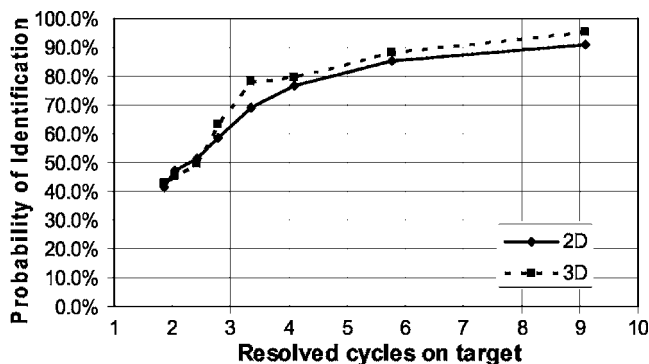


Fig. 7 Probability of object identification versus resolved cycles on target—all 10 observers.

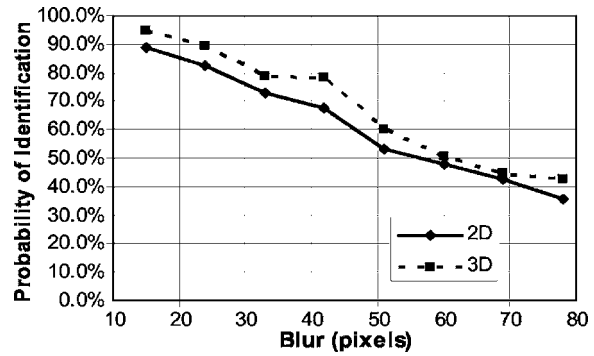


Fig. 8 Probability of object identification versus blur—6 observers with proven 3-D perception (3-D performance better than 2-D performance).

lation transfer function (MTF) from the blur described in Eq. (1) and the MTF of the monitor. The effective system CTF was the human contrast threshold function divided by the blur and monitor MTFs. An observer distance of 40 in. (101.6 cm) was measured and an average display luminance of 5 fL was obtained. The image size was 25.1 by 14.9 cm on the monitor. The average contrast of the targets was 0.23 and the average characteristic dimension was 114 pixels.

Figure 4 shows an example CTF of the system in the experiment. The blur associated with the eye is manifested in the human CTF. The spatial frequency given is associated with eye space. The dashed line shows how the limiting frequency is determined for a contrast of around 0.23. The point where the effective system CTF matches the target contrast gives the limiting frequency that can be seen across the target image. The number of cycles that can be resolved across the target dimension can be determined by multiplying the limiting frequency in cycles per milliradian by the characteristic dimension of the target in milliradians (i.e., pixels converted to milliradians in eye space).

The target contrasts were measured by segmenting the object and the background in the unblurred source images. Characteristic dimensions were developed from the square root of the object size in pixels and were converted to ob-

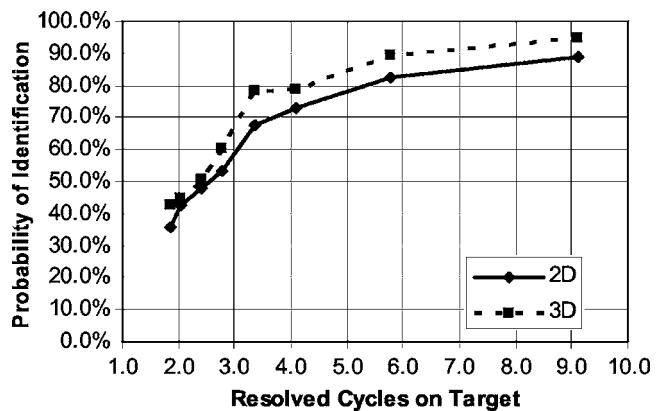


Fig. 9 Probability of object identification versus resolved cycles on target—6 observers with proven 3-D perception (3-D performance better than 2-D performance).

Table 3 Results summary for all 10 observers.

Resolved cycles on target	Blur width (pixels)	2-D	3-D	Difference (3-D-2-D)	
9.1	15	90.9%	95.0%	4.1%	
5.8	24	85.5%	88.2%	2.7%	
4.1	33	76.8%	79.5%	2.7%	
3.3	42	69.1%	78.2%	9.1%	
2.8	51	58.6%	63.2%	4.5%	
2.4	60	51.4%	49.5%	-1.8%	
2.0	69	47.0%	45.5%	-1.5%	
1.9	78	41.4%	42.9%	1.5%	
		65.1%	67.8%	2.7%	averages

server space using the monitor characteristics and viewing distance. Details of how to process the imagery and calculate the values and examples are given in Ref. 18. The resulting values for the ensemble of targets used in the experiment are provided in Table 2. The contrasts and characteristic dimensions/sizes (square root of total pixels) are averages for the 24 image set, which had front and side aspects for each of the 12 targets. The size is converted from linear image space in pixels to object space in milliradians and shown in the last column. These values were then used with the CTF/MTF curve, shown in Fig. 4, to determine the resolved cycles on target for each of the blur levels used in the experiment (and shown along the x axis of the results plots). The number of cycles that could be

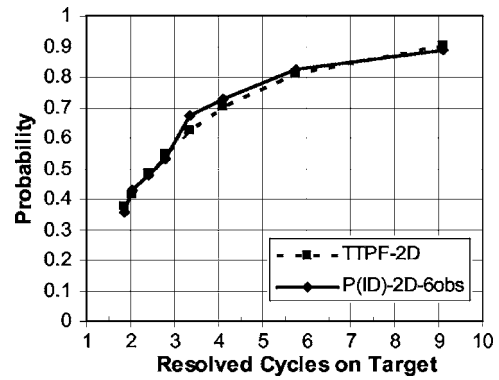


Fig. 10 Probability of ID (2-D) versus resolved cycles on target and the target transfer probability function curve for the model.

resolved on the objects at the blurs of 15, 24, 33, 42, 51, 60, 69, and 78 pixels were 9.1, 5.8, 4.1, 3.3, 2.8, 2.4, 2.0, and 1.9 cycles, respectively.

6 Perception Experiment (2-D/3-D Display)

Two orthogonally mounted mirrors allowed the simultaneous viewing of two monitors and provided the 3-D imagery capability. First surface mirrors were used to avoid ghosting effects for the observers.

The monitors used for the experiment were Cornerstone Color 50s, which were calibrated to provide the same contrast. The monitors were placed approximately 2 m apart (1 m from the central mirrors, as shown in Fig. 5) to reduce the distortions, which resulted in severe keystoneing at closer distances. The wrapping effects, visible at the shorter distances, were not as pronounced and were removed entirely by shrinking the buttons on the interface so they only occupied the width of the image plane.

To develop an impartial comparison for stereo versus single image experiment, several factors were taken into

Table 4 Results summary for observers with better 3-D than 2-D performance.

Resolved cycles on target	Blur width (pixels)	2-D	3-D	Difference (3-D-2-D)	
9.1	15	88.6%	94.7%	6.1%	
5.8	24	82.6%	89.4%	6.8%	
4.1	33	72.7%	78.8%	6.1%	
3.3	42	67.4%	78.0%	10.6%	
2.8	51	53.0%	59.8%	6.8%	
2.4	60	47.7%	50.8%	3.0%	
2.0	69	42.7%	44.5%	1.8%	
1.9	78	35.5%	42.7%	7.3%	
		61.3%	67.3%	6.1%	averages

Table 5 Range performance improvement.

	2-D	3-D
N_{50}	2.5	2.1
N_{90}	9.5	6.2

account. First, the images were presented in comparable resolutions for both the stereo and the 2-D case. In this experiment, the image size was accomplished purely by the construction of the stereo viewing apparatus. Two monitors were used and no truncation was performed on the images for display purposes (row interleaving, lenticular overlay, etc). This inherently allowed for both the stereo and 2-D images to be presented at the same resolution with no alteration. Subjects were also tested for stereo acuity before participating in the experiment. A series of pristine stereo images were presented to the observers to test their capabilities with regard to viewing stereo pairs. Time was also taken to allow the observers to adjust the viewing mirrors and monitors for optimum comfort and viewing.

The images were presented in a random fashion. That is, stereo and 2-D images were intermingled and both sets were viewed by the observer throughout the course of the test. Two different aspects were selected for each object, a front view and a side view. To minimize uncertainties, the same set of images (offset by different margins since four stereo pairs and five 2-D images were captured per target per aspect) were used in the test. This minimized uncertainties in analysis by removing uncertainties associated with differing levels of occlusion between differing levels of blur on stereo pairs of the same object.

7 Results and Analysis

The results from the observer perception experiments are presented in Figs. 6 and 7. Respectively, they are probability of identification as a function of blur in the image (directly analogous to range or resolution) and probability of identification as a function of resolved cycles on target. This second form is important, as this takes into account the target size and contrast presented to the observer, and

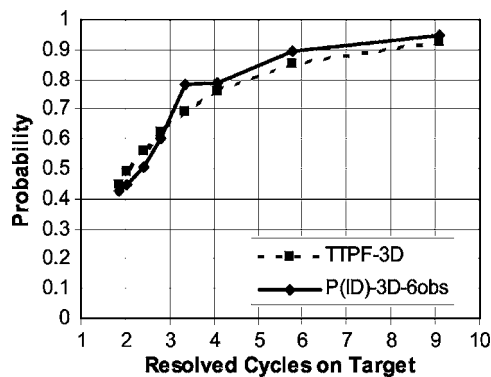


Fig. 11 Probability of Identification (3-D) versus resolved cycles on target and the target transfer probability function curve for the model.

Table 6 Results of 2-D range performance compared to previous work.

Experiment	N_{50}
MSS Passive Sensors Conf. 2003 ⁴	2.1
<i>Optical Engineering</i> paper ⁵	3.77
This effort	2.5

hence the independent variable is not experimental condition or setup-dependent. In other words, these results can be used by others.

It should be noted that there is an improvement in performance from 2-D to 3-D shown in Figs. 6 and 7. However, it is not a large improvement. This is especially the case if the improvement is interpreted to be an increase (“shifting up”) in the probability direction. This interpretation can be misleading. A more significant approach is to choose the 90% probability of correct identification line. While we calibrate the model performance using 50% probability, it is actually more meaningful to evaluate the improvement at 90%, which is a tactically relevant performance goal. The 2-D imagery, from Fig. 7, requires 8.5 resolved cycles on target to achieve 90% probability. The 3-D imagery, on the other hand, required 6.5 cycles on target to achieve 90% probability. This equates to a range performance improvement of approximately 30%, which is significant.

During the conduct of the experiment, it was noted by some observers that they had trouble perceiving the 3-D effects. These observers related that they only perceived it on what seemed to be a few of the images. As the experimental setup was not optimal for high-performance 3-D display, this result was foreseen prior to conducting the experiment. We had three available approaches to displaying 3-D imagery, and this one was evaluated as the best option for displaying 2-D and 3-D with the same resolution and display characteristics to enable direct comparison of the results. Consequently, the data was sorted according to performance to determine which observers did perceive 3-D consistently. Four of the 10 observers did not perform as well with 3-D as they did with the 2-D imagery. The data

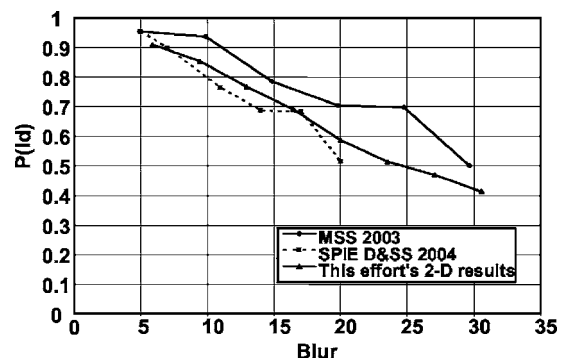


Fig. 12 Comparisons to previously reported results of probability of ID versus equivalent blur.

was additionally analyzed to look at just the results from the six observers with equal or better 3-D than 2-D performance. This is based on the premise that performing significantly worse at 3-D identification than 2-D identification indicated the observer's visual system was not reconciling the two views—he was seeing double and hence degrading his performance. These results are shown in Figs. 8 and 9. Like Figs. 6 and 7, Figs. 8 and 9 are probabilities of identification versus blur and resolved cycles on target, respectively.

The improvements in performance noted here are more significant than in the total data set, as expected. As all the observers were tested for depth perception, the fault is attributed to the hardware used to display the imagery and the experimental setup. One of the observers, a naval aviator and former intelligence imagery analyst, noted that he had used light tables and stereo intelligence displays (Joint Service Imagery Processing System) for imagery analysis/mensuration operationally and never had a problem perceiving depth using stereo pair imagery. In this case, however, he noted some difficulty.

These results are summarized in tabular format in Tables 3 and 4. These are for the entire observer ensemble and those that had better 3-D than 2-D performance (6 of 10).

The performance curves from the probability of identification in both 2-D and 3-D cases were used to determine the N_{50} results for use in a target transfer probability function (TTPF). The TTPF used in this case is given in Eq. (2). This type of equation is used with the ACQUIRE model methodology in field performance by wargaming modelers when running engagement analyses. A minimum mean-squared-error methodology was used to determine the N_{50} for this case. The resulting curves are shown in Figs. 10 and 11, for the ensemble of six observers with good 3-D performance, for the 2-D and 3-D cases, respectively. Additionally, the improvement in range performance is summarized in Table 4. The summary result shown in Table 5 is approximately a 30% improvement in range performance for the 90% probability of identification case.

$$P_{ID}(N) = \frac{(N/N_{50})^{1.73}}{1 + (N/N_{50})^{1.73}} \quad (2)$$

These results shown in Table 5 were compared with the results from those previously reported.³⁻⁵ This comparison is shown in Fig. 12 and Table 6. The 2-D data from this experiment was used. There was a significant difference between N_{50} noted. Subsequent investigation revealed that the Military Spectral Sensing (MSS) conference paper⁴ effort and this paper's effort both segmented and defined the target as the object and any portion of the fingers or hand that overlapped the object. The SPIE Defense & Security (D&S) 2004 conference paper³ defined the object to include the hand up to the wrist. The resulting characteristic dimensions are larger, hence the N_{50} values reported are larger. A check of the relative sizes/ N_{50} values shows that they are essentially equivalent. Either method of defining the target works; as long as the engineer uses the larger N_{50} of 3.8 and includes the hand to the wrist or the smaller N_{50} and just the object dimensions, the resulting predictions are the same. The MSS 2003 effort⁴ used only the object (not the hand) for determining critical dimension. The slightly

lower number (2.1 versus 2.5) is accounted for as this was a different set of handheld objects, which were slightly easier to discriminate. The set used in this experiment is nearly identical to the set of objects used in the D&S 2004 conference paper.³

8 Conclusions and Future Efforts

In conclusion, we believe the results indicate 3-D imagery can provide significant improvement in range performance for the identification of threat objects held in a single hand. The results presented here may prove to be useful in evaluating the desirability of adding the third dimension to imagers for MOUT or AT/FP applications.

There were significant indicators that the performance of our display architecture prevented some of the observers from perceiving the benefit of 3-D imagery. Initial indications are that further time and resources should be invested to examine the issue in more detail. However, the results reported here show that there are some benefits associated with 3-D imaging. Further experimentation is required to quantify the benefits associated with different architectures.

Acknowledgment

One of the authors (CH) gratefully acknowledges support of the Army's Night Vision and Electronic Sensors Directorate, EOIR Technologies, the Army Research Laboratory under grant W911NF-05-2-0019, the Office of Naval Research under grant N00014-05-1-0446, and the Army Research Office under grant W911NF-05-1-0307.

References

1. B. Stann, K. Aliberti, D. Carothers, J. Dammann, G. Dang, M. Giza, W. Lawler, B. Redman, and D. Simon, "A 32×32 pixel focal plane array lidar system using chirped amplitude modulation," in *Laser Radar Technology and Applications IX*, G. W. Kamerman, Ed., *Proc. SPIE* **5412**, 264–272 (Sep. 2004).
2. J.-C. Kastelik and M. Gazelet, "Stereoscopic displays," in *Encyclopedia of Optical Engineering*, Marcel Dekker, New York (2003).
3. S. K. Moyer, E. Flug, T. C. Edwards, K. A. Krapels, and J. Scarborough, "Identification of handheld objects for electro-optic/FLIR applications," in *Infrared Imaging Systems: Design, Analysis, Modeling, and Testing XV*, *Proc. SPIE* **5407**, 116–126 (Aug. 2004).
4. S. Moyer, R. Driggers, D. Wilson, G. Welch, and W. Rhodes, "Cycle criteria for fifty-percent probability of identification for small handheld objects," *Proc. Military Sensors Symposium, Passive Sensors* (2003).
5. S. Moyer, J. Hixson, T. Edwards, and K. Krapels, "Probability of identification of small handheld objects for electro-optic/FLIR applications," *Opt. Eng.* **45**, 063201 (2006).
6. J. Ratches, R. Vollmerhausen, and R. Driggers, "Target acquisition performance modeling of infrared imaging systems: past, present, and future," *IEEE Sens. J.* **1**(1) 31–40 (June 2001).
7. R. Driggers, P. Cox, and T. Edwards, *Introduction to Infrared and Electro-optical Systems*, Artech House, Boston, MA (1999).
8. J. Leachtenauer and R. Driggers, *Surveillance and Reconnaissance Imaging Systems*, Artech House, Boston, MA (2001).
9. J. Johnson, "Analysis of image forming systems," *Proc. Image Intensifier Symp.* pp. 249–273 (1958).
10. M. C. Dudzik, "Electro-optical systems design, analysis, and testing," *The Infrared and Electro-Optical Systems Handbook*, Vol. 4, Environmental Research Institute of Michigan, Ann Arbor, MI (1993).
11. J. A. Ratches et al., "NVL static performance model for thermal viewing systems," USA Electronics Command Report ECOM 7043, AD-A011212 (Apr. 1973).
12. J. A. Ratches, "Static performance model for thermal imaging systems," *Opt. Eng.* **15**(6), 525–530 (Dec. 1976).
13. J. A. Ratches, "Comparison of NVL model and four contractor models for minimum resolvable temperature (MRT)," USA Electronics Command Report ECOM 7050, AD-A024467 (Jan. 1976).
14. J. A. Ratches, "NVL modeling: historical perspective," in *Infrared Imaging Systems, Analysis, Modeling and Testing X*, *Proc. SPIE* **3701**, 1–12 (1999).

15. W. R. Lawson and J. A. Ratches, "Modeling detection or the detection game," *Proc. IRIS Specialty Group on Targets, Backgrounds and Discrimination*, Institute for Defense Analyses, Arlington, VA (Aug. 1980).
16. J. A. D'Agostino et al., "ACQUIRE range performance model for target acquisition systems version 1 user's guide," USA CECOM Night Vision & Electronic Sensors Directorate Report, Fort Belvoir, VA (May 1995).
17. J. A. Ratches, R. Vollmerhausen, and R. Driggers, "Target acquisition performance modeling of infrared imaging systems: past, present, and future," *IEEE Sens. J.* **1**(1) 17-42 (June 2001).
18. R. Vollmerhausen, "Incorporating display limitations into night vision performance models," *IRIS Passive Sensors 1995*, Vol. 2, pp. 11-31 (1995).
19. L. M. Biberman, Ed., *Electro-Optical Imaging: System Performance and Modeling*, Chap. 12, SPIE Press, Bellingham, WA (2000).
20. N. A. Dodgson, "Variation and extrema of human interpupillary distance," in *Stereoscopic Displays and Virtual Reality Systems XI*, *Proc. SPIE* **5291**, 36-46 (2004).
21. W. R. Watkins, D. H. Tofsted, V. G. CuQlock-Knopp, J. B. Jordan, and J. O. Merritt, "Navigation through fog using stereoscopic active imaging," in *Enhanced and Synthetic Vision*, *Proc. SPIE* **4023**, 20-28 (2000).



Keith Krapels has been a program officer in the Surveillance, Communications and Electronic Combat Division at the Office of Naval Research since fall of 2001. From 1999 to 2001, he was a senior electrical engineer in the Sensor Performance Model Development Branch at the U.S. Army Night Vision and Electronic Sensors Directorate. His work included electro-optical/infrared (EO/IR) sensor modeling, analysis, and testing. From 1996 to 1998 he worked as special projects engineer in the Tactical Electronic Warfare Division of the Naval Research Laboratory. From 1990 to 1996, he was an electronic warfare officer in U.S. Navy EA-6B aircraft. From 1987 to 1989, he worked as an EO/IR sensor systems analyst at Martin Marietta Orlando Aerospace, as a research fellow at the U.S. Air Force Arnold Engineering Development Center, and as a research associate at the University of Memphis.



Ronald G. Driggers received a doctorate in electrical engineering from the University of Memphis in 1990. Dr. Driggers has 19 years of electro-optics experience and has worked for or consulted to Lockheed Martin (Orlando), SAIC, EOIR Measurements, Amtec Corporation, Joint Precision Strike Demonstration Project Office, Redstone Technical Test Center, and Army Research Laboratory. He is currently the director of the Modeling and Simulation Division at the U.S. Army's Night Vision and Electronic Sensors Directorate

(NVESD). Dr. Driggers is the author of three books on infrared and electro-optics systems and has published over 80 papers. He is editor of Marcel Dekker's *Encyclopedia of Optical Engineering* and was an associate editor of *Optical Engineering*. He was selected as the 2002 Army Materiel Command's Engineer of the Year and was selected in the Top 10 2002 Federal Engineers of the Year. He is a U.S. Naval Reserve Officer and was selected as the 2001 Engineering Duty Officer of the Year (William Kastner Award). He is also a Fellow of SPIE.

Brian Teaney: Biography and photograph not available.



Carl Halford is the First Tennessee University Professor in Electrical and Computer Engineering at the University of Memphis, where he is also director of the Center for Advanced Sensors. He received the PhD degree from the University of Arkansas, Fayetteville, in electrical engineering. His research interests include modeling of imaging sensors, laser illuminated imaging, infrared sensors, electro-optical systems testing, and uncertainty analyses. Summer/consulting experience includes work with EOIR Technologies and the Army's Night Vision Laboratory, the Army's Redstone Technical Test Center, Lockheed Martin Orlando, Analytical Systems Engineering Corporation, the Army Missile Command at Redstone Arsenal, NASA's Johnson Space Center, and Avco Everett Research Laboratory. Dr. Halford is a Fellow of SPIE, a senior member of the IEEE, and a member of the OSA.